Journal of Ovonic Research Vol. 11, No. 3, May - June 2015, p. 113 - 121

STUDY OF MORPHOLOGY FORMATION OF NEAR THRESHOLD PERCOLATING METALLIC NANOPARTICLE THIN FILMS SHOWING NON-OHMIC BEHAVIOR

A. SATTAR[a,b], R. J. AMJAD[a], H. MAHMOOD[a], M. NIAZ AKHTAR[a], H. LATIF[c], M. KHALID[d], A. USMAN[a], M. IMRAN[a], A. IQBAL[a*]

[a]*Department of Physics, COMSATS Institute of Information Technology, Lahore 54000, Pakistan*

[b]*MacDiarmid Institute for Advanced Materials and Nanotechnology, Department of Physics and Astronomy, University of Canterbury, Christchurch 8140, New Zealand*

[c]*Department of Physics, Forman Christian College Lahore Pakistan*

[d]*Department of Physics, NED University of Engineering and Technology, Karachi, 75270, Pakistan*

Nanoparticles produced by inert gas aggregation system were deposited on the Silicon Nitride (Si_3N_4) substrates under good vacuum conditions. Nanoparticles coalesced and agglomerated rapidly as they were deposited on the substrate. A peculiar voltage dependent non-ohmic conductance behavior was observed for certain film morphologies, whereas the resultant morphology of these films was found to be dependent upon the initial size of particles, deposition rate and the ambient conditions of the films. The coalescence enhanced, due to large deposition rate or low oxidation rate, played a vital role in the formation of metallic films in large islands separated by cracks and voids suitable for conductance switching behavior. Simulations were performed to mimic and understand the morphology of these experimentally produced films. A new improved model is presented in which coalescence was restricted by deposition rate and maximum size limit of the particles formed by coalescence. Initial and cut-off sizes of particles along with a new parameter which is directly proportional to the deposition rate were used for our simulations. By varying these parameters, a range of simulated morphologies were generated for a successful comparison with experimental results and for the indirect calculation of the oxidation time after which the particles stop coalescing.

(Received April 1, 2015; Accepted May 22, 2015)

Keywords: Simulations, Nanoparticles, Coalescence, Percolation, Oxidation, Conductance switching

1. Introduction

Percolating thin films of metallic nanoparticles have been of great interest due to their unique electrical properties [1-2]. Interesting new applications have been suggested for percolating films such as gas sensors [3-6], fuel cells [7-9] and memory devices showing memristive behavior [11]. Surface morphology of thin films defines many of the electrical transport properties which are fundamental to the applications mentioned above.

In this work experimental results are presented for inert gas aggregated metallic (Tin (Sn) and Lead (Pb)) nanoparticles deposited on Si_3N_4 substrates along with the computer simulations. These metallic particles coalesce readily under good vacuum conditions [12] which alters the film morphology. Moreover, the rate of coalescence is directly dependent on oxidation of the nanoparticles surfaces which slows the coalescence rate drastically [12]. Coalescence of individual particles size ranging from few nanometers to few microns has been studied in the past [13-15].

* Corresponding author: azmatiqbal786@gmail.com

The properties of percolating films critically depend upon the final film morphology. Due to coalescence, the film morphology varies continuously during and after the deposition. Smaller particles coalesce and form larger particles and hence changing the effective coverage of the film. Also the structure of the connected particles changes with the passage of time due to coalescence. We have studied the effect of coalescence on film by comparing experimental results to a proposed model simulated using computer. In our simulations particles were landing on a substrate one by one. The deposition was continued until a percolating path was formed by the particles. Morphologies of percolating thin films generated by simulations were then compared to the experimentally produced thin films.

2. Methods and Techniques

2.1 Inert Gas Aggregation System

Thin films of Tin (Sn) nanoparticles were fabricated using a high vacuum compatible Inert Gas Aggregation system. The source chamber consists of a DC magnetron sputter source housed in a liquid nitrogen cooled aggregation chamber. A continuous flow of inert gases such as Argon and/or helium is maintained in the aggregation chamber to assist the formation of nanoparticles in gas phase. The details of this system can be found elsewhere [16]. Nanoparticles of ~7 nm diameter were deposited onto a Si/Si_3N_4 with prefabricated gold electrodes for in-situ electrical measurements.

During the deposition process a constant voltage was applied to the electrodes and the electrical current was continuously recorded. Fig. 1 shows the evolution of electrical behavior of nanoparticle films during the deposition. An onset of high current indicates the formation of a conducting path between the electrodes. This happens when the coverage is high enough for the formation of a percolating cluster of nanoparticles. This sharp increase in current is used as an indicator of the percolation threshold and the deposition was stopped using a pneumatic valve which isolates the deposition chamber from source chamber. Pressure was kept in 10^{-6} torr range during the deposition. Later on the deposition chamber was vented and samples were taken out for SEM analysis.

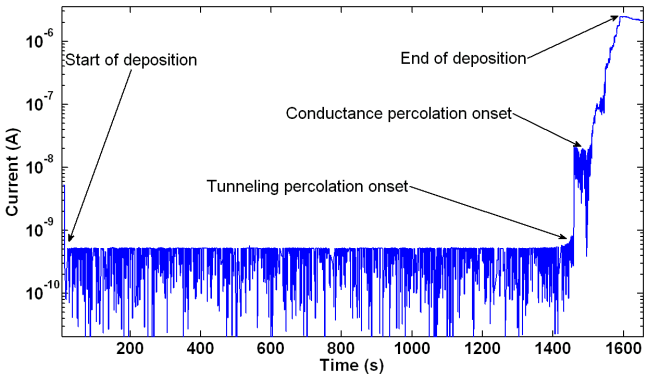

Fig. 1 In-situ electrical measurements showing onset of high current at the point of percolation threshold

2.2 Computational Simulations

To understand the formation of nanoparticle thin films and the percolation phenomenon, a computational model was developed using Matlab. Deposition of nanoparticles was simulated by introducing new spherical particles of fixed diameter of 7nm at random location on the initially empty substrate. For simplicity atomic arrangement was considered to be simple cubic.

In the past, morphological changes due to coalescence have been studied by simple models such as Family and Meakin Model (FMM[17]) and interrupted coalescence model (ICM[18]). FMM allows coalescence to all the particles that come in contact at any stage. On the other hand ICM restricts coalescence of the particles that are above certain critical radius.

In our model we have included the effect of deposition rate to satisfy the dynamic nature of thin film morphologies produced using IGA systems. As the deposition starts, incoming particles land one by one on the substrate surface. Every new coming nanoparticle could land either on the empty space of the substrate or on the already deposited nanoparticles. Also the landing particle could touch one or more already deposited particles. The deposited metallic nanoparticles in contact to each other tend to coalesce and agglomerate. The coalescence process was simulated by replacing the touching particles with a new single particle with volume equal to combined volume of replaced particles. The radius of new particle (R_c) formed after coalescence is given by:

$$R_c = \left(R_i^{\,3} + \sum_k R_k^{\,3}\right)^{\frac{1}{3}} \tag{1}$$

where

R_c=Radius of the new particle produced by coalescence of the touching particles

R_i=Radius of the latest particle deposited

R_k =radius of the k^{th} touching particle

The nanoparticles deposited much earlier could have been oxidized due to oxygen present in the deposition chamber and thus do not coalesce due to hard oxide shell around them [12]. To simulate this effect for coalescence we only considered last n deposited particles. Here n is equal to the number of the consecutively deposited particles before the current particle that were considered to be active for coalescence (for a unit area). Also coalescence is restricted by an upper limit to the radius of the resultant particles after coalescence, i.e., the coalescence will only occur if the coalesced particle is smaller than the provided upper limit of size.

In our simulation, by changing n, we could decide the time span for which the particles remain active for coalescence, i.e., not having enough oxidation to hinder the process of coalescence with new particles. The time after which the particles will no longer coalesce is termed as oxidation time (t_{ox}) in this text. The relation of oxidation time ($\boldsymbol{t_{ox}}$) and deposition rate (N) to the parameter n is:

$$t_{ox} = \frac{n}{N} \tag{2}$$

In the experiments we can control the parameter n by varying either or both the deposition and oxidation rate. Controlling oxidation rate is not feasible in our experiments, however, controlling deposition rate is possible by varying the conditions and parameter of source chamber such as sputter power, inert gas flow rate and aggregation length etc.

Distributive computing was used to improve the speed of the simulation. Algorithm for producing deposition is shown in Fig. 2. Input parameters such as deposition rate, particle size and substrate size were passed to each node/workers. Each worker then produced samples in parallel to speed up the simulations. Matrices were initialized as zero matrices representing empty substrates. Touching particles were detected after adding each new particle to the substrate. All the touching particles not older than n were merged together to simulate coalescence. In the next step, substrate was tested for percolation. Once the percolating sample was achieved, deposition was stopped and the results were saved to the disk for subsequent analysis.

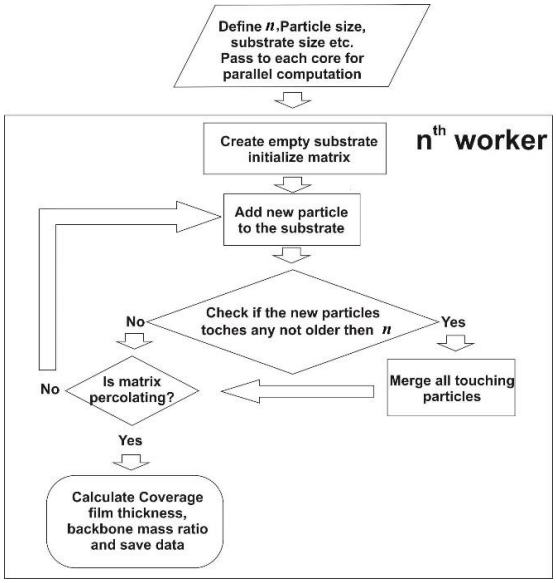

Fig.2 Algorithm for computer simulations of nanoparticle thin films showing coalescence effect.

3. Results and Discussion

3.1 Experimental results

The morphologies of thin films produced using IGA systems are totally different from morphologies produced by other methods such as physical sputtering and thermal evaporation. In contrast to atom by atom deposition, IGA system produces nanoparticles which are deposited on the substrate as building blocks of the thin films. Fig. 3 shows comparison of two metallic thin films deposited using thermal evaporator (Fig. 3(a)) and IGA source (Fig. 3(b)). It can be clearly seen in the SEM micrograph cross-section view that the films deposited using thermal evaporator are much smoother and homogeneous compared to the film deposited using IGA. Discrete, island-like structures are visible in Fig. 3(b) formed due to the coalescence of individual incoming nanoparticles.

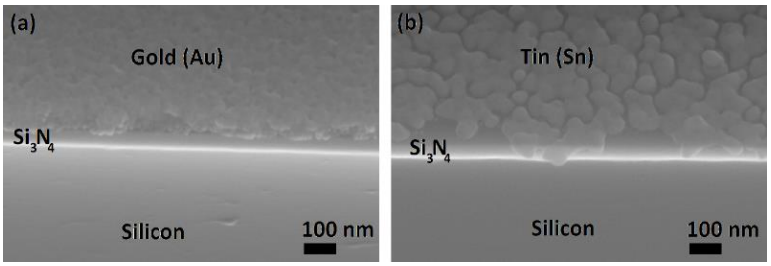

Fig. 3 Cross-section view of different morphologies of metallic films deposited using (a) thermal evaporator, (b) Inert Gas Aggregation System showing island like structures formed due to coalescence between incoming clusters.

The morphology of the films varied as we changed the deposition conditions. Presence of oxygen or nitrogen in the source chamber greatly affects the properties of particles being produced. The cluster coalesce differently and form diverse morphologies for different source conditions such as oxygen/nitrogen concentrations [19]. The fundamental reason of variation in coalescence is the formation of oxide layer around the

Sn nanoparticles which acts as a hard shell prohibiting coalescence between the particles inside the deposition chamber. Fig. 4(a) shows TEM results of an experimentally produced Sn cluster thin film. Agglomerated and coalesced islands of few tens of nanometer are clearly visible in TEM images. Color contrast of various areas of the film indicate amount of material in certain regions. Darker areas represent thicker islands. A 3D surface plot is generated for this TEM image using image contrast. 3D rendering of TEM shown in Fig. 4(b) shows coalescence in the deposited particles. There are particles which fully coalesce and form bigger particles with larger diameter and hence contributing lesser to the areal coverage compared to the particles which do not coalesce fully (labelled as 'overlapping particles' in the Fig. 4(b)). This explains the trend of increase in mean film thickness as n is increased (i.e. increase in coalescence) shown in Fig. 4(b).

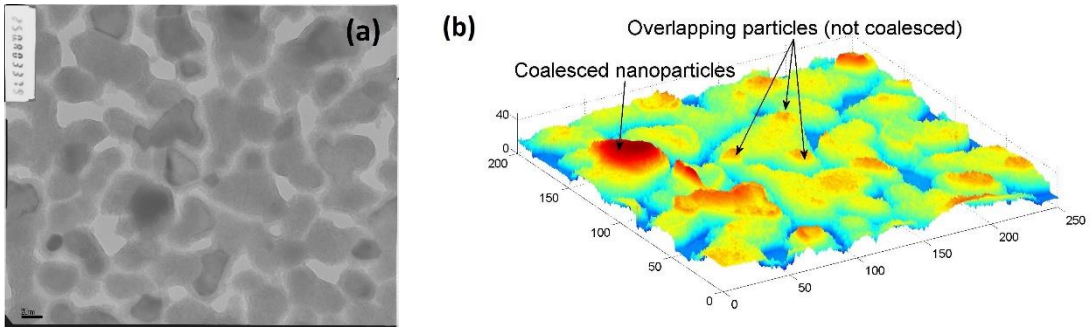

Fig. 4 (a) TEM image showing islands formed by agglomerates and coalesced nanoparticles. (b) A 3 dimensional rendition of TEM image shows higher islands are formed where incoming particles are overlapped.

During the course of experiment 196 samples of Sn nanoparticle films were prepared. All the samples were then divided into four categories (A, B, C and D) according to the conduction onset behavior at percolation threshold (see Fig.5). All the samples showing smooth onsets were categorized as 'A', whereas the samples showing steps of the order of 1, 5 and 10 G_0 (where $G_0=2e^2/h$) in their conductance onset were categorized as 'B', 'C' and 'D' respectively.

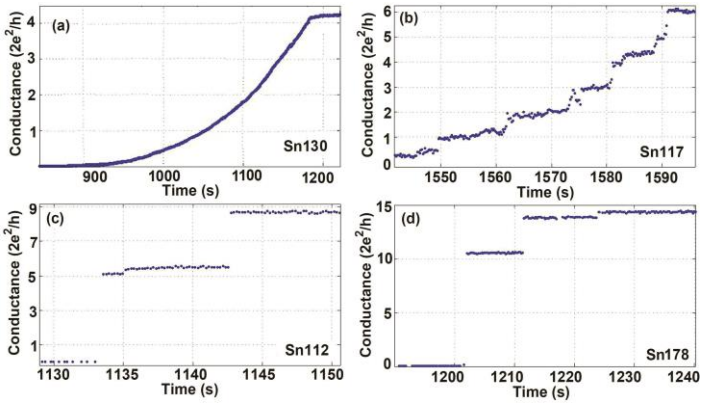

Fig.5 Typical onset of electrical conduction at percolation threshold used to define categories A-D.

The samples in category 'B' showed peculiar switching effects. Two terminal devices with lithographically defined gold electrodes and percolating thinfilms were tested under varying applied voltages as shown in the Fig.6.

As the voltage gradually increases from zero to a peak voltage of 3 V, sample conductance jumps abruptly to higher values. However, the conductance jumps back to lower values as the voltage sweeps continues. The cycle of increase and decrease in conductance continues with the voltage cycle. This interesting behavior is only observable for a certain morphologies.

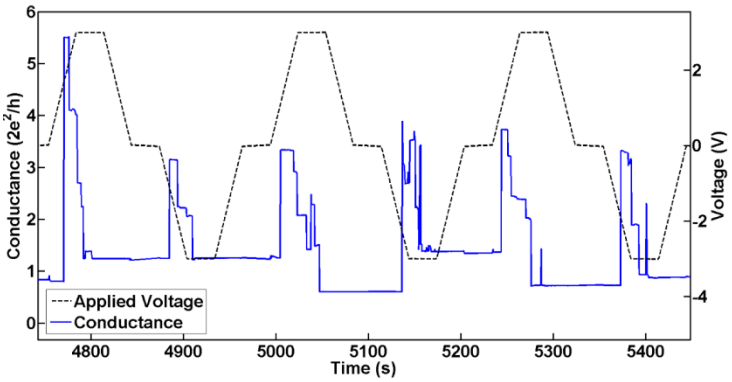

Fig.6 Effect of applied voltage (dashed lines) on the conductance of the film (solid lines). Conductance jumps to higher values during the increase in applied voltages. The conductance jumps back to lower values as the sweep in voltage continues.

The SEM micrograph for typical samples out of these categories are shown in the Fig.7. It can be seen clearly that the morphology of the film is different for each category. Samples from category 'A' show lowest coalescence while category 'D' samples showed highest coalescence. In terms of coalescence category 'B' and 'C' lies in between of those of 'A' and 'D'. It was observed that the critical film thickness of each category depends upon the deposition rate used. The comparison of these experiments with simulation is presented in the next section.

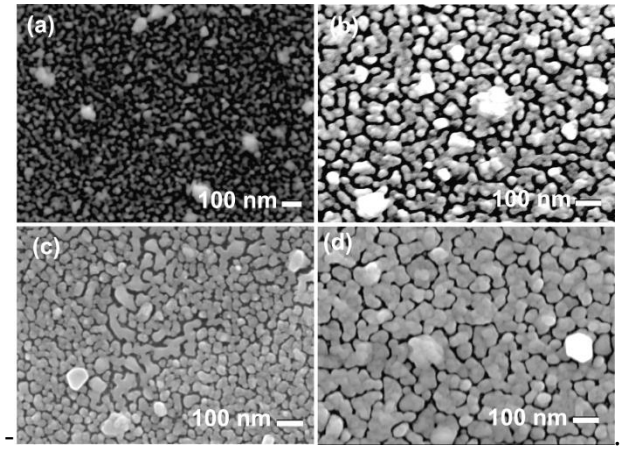

Fig. 7 SEM images showing typical morphology of samples from category A-D.

3.2 Comparison of Experimental and Simulation Results

First we discuss the comparison of the morphologies produced by experiments and simulations. Simulations were run for ten different *n* ranging from 0 to 70 for particle of diameter 7 nm with the substrate size of 100 nm. The deposition was continued until the percolation threshold was reached. 100 simulated samples were produced for each deposition rate. Simulated film morphologies were produced for the parameters such as deposition rate and incoming particles sizes. Comparison of SEM of experimentally deposited films with simulated

morphologies provides an excellent insight for the phenomenon governing the formation of different film structures. Nanoparticles produced in IGA systems produced percolating films with morphologies ranging from filament like structures to highly coalesced islands. Here we discussed three extreme cases that have been observed for experimentally deposited films using IGA systems. Fig. 8(a), (c) and (e) show SEM images of filament like structure, isolated particles and highly coalesced island structures respectively. All these different morphologies were produced under controlled parameters such as deposition rate and average particle size. By changing these input parameters a variety of resultant thin film's structures can be obtained. However, study of the physical processes behind the formation of final structures after the deposition of nanoparticles on the substrate cannot be directly observed. Our initial simulations provide a glimpse of what might be the reason of formation of such variety of structures in metallic cluster thin films.

In the experiments, filament like structures were produced when the particle size was ~60 nm in diameter (Fig. 8(a)). In simulations similar morphologies were attained when smaller *n* were selected along with 60 nm diameter particles (Fig. 8(b)). Another type of morphology was observed in experiments where the particles do not coalesce and very small or no islands are visible in SEM image (Fig. 8(c)). In the simulations when the particle size was 15 nm and deposition rate was very low (n~1) then the nanoparticles maintained their integrity during the deposition (Fig. 8(d)). This could have happened when in actual experiments the clusters got oxidized right after the deposition before any of other incoming nanoparticles were deposited on top of it. The reason for this could be either one or a combination of the following three:

1) Very slow deposition rate with minute oxidation.
2) High oxidation rate in deposition chamber.
3) Oxidation in source chamber of IGA (which could be the reason of slow deposition rate at the first place).

Finally Fig. 8(e) shows the morphology having highly coalesced films. In simulations (Fig. 8 (f)) the highly coalesced island structures were obtained when the deposition rate parameter was selected to be higher (n =10) along with bigger diameter of the incoming particles (40 nm).

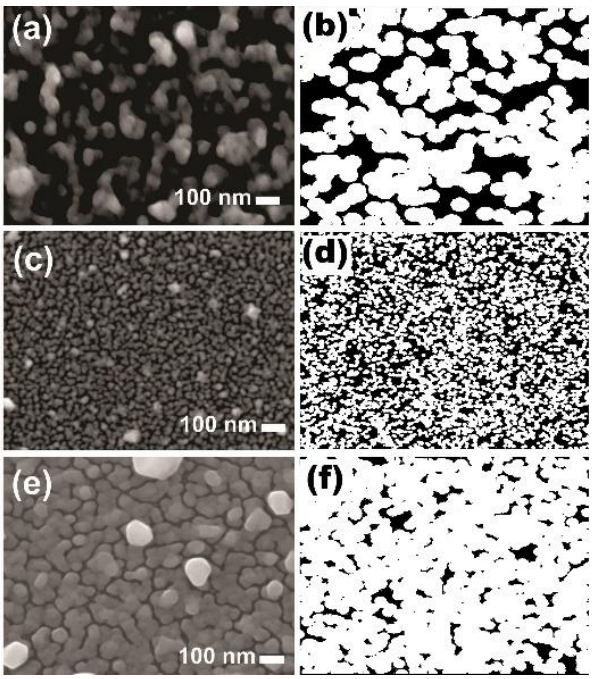

Fig.8 SEM micrographs of nanoparticle films showing (a) minute coalescence with 60 nm diameter incoming particles (b) minute coalescence with 60 nm diameter particles (c) 15 nm diameter particles with huge coalescence. On the right side (b, d and f) show corresponding simulated film morphologies for comparison.

The formation of cracks and voids only resemble partially with our simulated results. The long range cracks spreading all over the films as seen in the SEM (Fig. 8 (e)) are not produced by instant coalescence between the incoming particles. The cracks must have appeared later due to reordering in the percolating this films due to subsequent coalescence within the islands formed due to inter-particle coalescence.

For the categories mentioned in previous section, the average critical film thickness was calculated where a percolating path is formed between the electrodes for each sample. It was found that the average critical thickness increases with the increase in the deposition rate which indicates the existence of a correlation between deposition rate and the critical film thickness (see Fig. 9). This trend is similar to the trend of coalescence in categories A-D as evident from SEM results (Fig. 7). In short deposition rate, coalescence and critical thickness are interconnected in these particle film deposited by IGA systems. A comparable trend was observed for the simulation results from our model. Critical thickness obtained from experiments and simulations were compared. It can be seen from the Fig. 9 that the values are similar when *n* was selected between 30 and 40 and the upper limit of particle diameter was 25 nm.

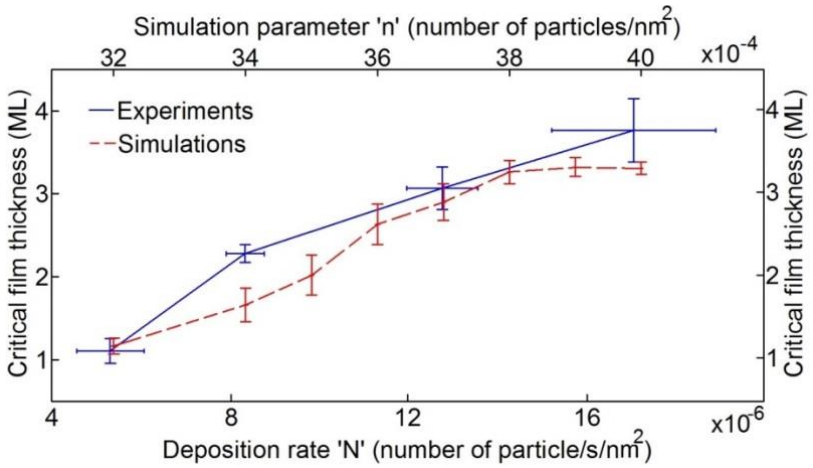

Fig. 9 Correlation of film thickness to achieve percolation threshold and deposition rate. Solid line: Each point (A-D) represents a data set of multiple sample, 196 samples in total. Vertical and horizontal error bars represent standard deviation in film thickness and deposition rates respectively. Dashed line: Simulation results are also shown along showing similar trend to that of experimental results.

Fig. 9 shows an increase in average critical film thickness as the deposition rate is increased. When a lower deposition rate is selected (i.e. lower amount of coalescence) the incoming particles retain their individuality. The incoming particles that fall on previously deposited particles keep mounting on each other (overlapping) instead of forming a larger coalesced island. A higher number of particles are then needed to increase the effective surface coverage as more and more particles are wasted due to overlapping at lower deposition rates. This trend continues until *n* reaches a value ~38, after that the critical film thickness reaches its saturation point. The average oxidation time t_{ox} after which a certain particle becomes inert to any further coalescence can be calculated using Equation (2) and in our case it is found to be of the order of 350 s for Sn nanoparticle thin films.

4. Conclusions

Percolating thinfilms formed with metallic clusters can be categorized according to their onset electrical behavior. Samples with step like onset electrical signature show voltage dependent non-ohmic conductance. The morphologies of such films were further studied using SEM and TEM analysis. Computer simulations using deposition rate and particle size as basic parameters

were successfully performed to mimic the SEM results of experimentally deposited metallic cluster thin films. The deposition rate and the critical film thickness were found to be correlated. The experimental results showed that when the deposition rate is higher the critical thickness required for percolation is also higher and vice versa. Similar results were found in computer simulations. Three distinct structures observed in experiments, i.e. Filament like structure, isolated particles and highly coalesced island structures were reproduced using simulations. It was found that the first two of above mentioned structures are formed when the deposition rate is slower (coalescence rate being negligible) and the particle sizes are 60 nm and 15 nm respectively. The highly coalesced structures were formed when the deposition rate was higher (i.e. higher chances of coalescence) and the size of particles was around 40 nm. Further improvements in the model can be achieved by considering other important aspects in formation of film morphology such as wetting angle, partial coalescence (forming dumbbell and ellipsoids). Better understanding of these thin films will provide better control while using these percolating as switching memory and other related applications.

Acknowledgments

Authors are highly grateful to Prof. Simon Brown and The New Zealand Foundation for Research, Science and Technology for providing laboratory facilities for experiments and computing support.

References

[1] X. Zhang, D. Stroud, Phys. Rev. B **9**, 2131(1995)
[2] V. V. Sysoev, J. Goschnick, T. Schneider, E. Strelcov, A. Kolmakov Nano Lett. **7**, 3182(2007)
[3] V. Arivazhagan, S. Rajesh, J. Ovonic Res. **6,** 221(2010)
[4] J. Dräger, S. Russ, T. Sauerwald, C. Kohl, A. Bunde, J. Appl. Phys. **113,** 223701(2013)
[5] M. Ulrich, C. Kohl, A. Bunde, Thin Solid Films **391**,299(2001)
[6] M. Ulrich, A. Bunde, A. Kohl, App. Phys. Lett. **85,** 242(2004)
[7] D. Chen, Z. Lin, H. Zhu, R. J. Kee, J. Power Sources **191**,240(2009)
[8] A. Bertei, C. Nicolella, Journal of Power Sources **196**, 9429(2011)
[9] L. C. R. Schneider, C. Martin, Y. Bultel, L. Dessemond, D. Bouvard, Electrochim. Acta **52**, 3190(2007)
[10] A. S. Martinez, J. Brouwer, Electrochim. Acta **53**, 3597(2008)
[11] A. Sattar, S. Fostner, S. A. Brown, Phys. Rev. Lett. **111**, 136808(2013)
[12] P. Y. Convers, D.N. McCarthy, A. Sattar, F. Natali, S. C. Hendy, S. A. Brown, Phys. Rev. B **82,**115409(2010)
[13] G. C. Kuczynski, J. Appl. Phys. **20**, 1160(1949)
[14] J. R. Blachere, A. Sedehi, Z. H. Meiksin, J. Mater. Sci. **19**, 1202(1984)
[15] T. Hawaa, M. Zachariaha, Aerosol Sci. B **37,** 1(2006)
[16] R. Reichel, J. G. Partridge, A. D. F. Dunbar, S. A. Brown, O. Caughley, A. Ayesh, J. Nanopart. Res. **8,**405(2006)
[17] F. Family, P. Meakin, Phys. Rev. Lett. **61,**428 (1988)
[18] X. Yu, P. M. Duxbury, G. Jeffers, M. A. Dubson, Phys. Rev. B **44**, 13163 (1991)
[19] T. F. Watson, D. Belic, P. Y. Convers, E. J. Boyd, S. A. Brown, Eur. Phys. J. D **61**, 81(2011)
[20] M. Massachi, J. Appl. Phys. **48**, 1408 (1977)
[21] A. Ofir, S. Dor, L. Grinis, A. Zaban, T. Dittrich, J. Bisquert, J. Chem. Phys. **128**,064703(2008)
[22] S. Roy, R. Chatterjee, S. B. Majumder, J. Appl. Phys. **110**, 036101(2011)